

Verification of gyrokinetic particle simulation of current-driven instability in fusion plasmas. III. Collisionless tearing mode

Dongjian Liu,^{1,2} Jian Bao,³ Tao Han,¹ Jiaqi Wang,¹ and Zhihong Lin^{4,a)}

¹College of Physical Science and Technology, Sichuan University, Chengdu 610064, People's Republic of China

²Southwestern Institute of Physics, Chengdu 610041, People's Republic of China

³Fusion Simulation Center, Peking University, Beijing 100871, China

⁴Department of Physics and Astronomy, University of California, Irvine, California 92697, USA

(Received 17 November 2015; accepted 18 January 2016; published online 5 February 2016)

A finite-mass electron fluid model for low frequency electromagnetic fluctuations, particularly the collisionless tearing mode, has been implemented in the gyrokinetic toroidal code. Using this fluid model, linear properties of the collisionless tearing mode have been verified. Simulations verify that the linear growth rate of the single collisionless tearing mode is proportional to D_e^{-2} , where D_e is the electron skin depth. On the other hand, the growth rate of a double tearing mode is proportional to D_e in the parameter regime of fusion plasmas. © 2016 AIP Publishing LLC.

[<http://dx.doi.org/10.1063/1.4941094>]

I. INTRODUCTION

The tearing mode is a dangerous current-driven magneto-hydrodynamic instability in magnetized plasmas.^{1–3} It may destroy the topology of the equilibrium magnetic field and lead to severe transport of plasmas from the core to the boundary of magnetically confined plasmas in a tokamak. The tearing mode in the tokamak core is believed to be responsible for the major crash.^{4–6} In the boundary region, such as the plasmas pedestal of a tokamak in H-mode discharges, the micro-tearing mode is suspected to be responsible for anomalous transport of electrons in high-beta plasmas.^{7–10} Nonlinearly, there are strong couplings between the tearing mode and other plasma modes, such as Alfvén waves and drift waves. The tearing mode-induced magnetic islands change the shape of continuous spectrum and the gap structure of shear Alfvén waves,^{11,12} which then influence the behavior of Alfvén eigenmodes such as toroidal Alfvén eigenmode (TAE) and beta-induced Alfvén eigenmode (BAE).^{13,14} Furthermore, the tearing mode can modify the equilibrium pressure profile of tokamak plasmas. Inside the magnetic island, the pressure tends to flatten, which decreases the drive for the drift waves such as ion or electron temperature gradient modes. Near the boundary of the magnetic island, the pressure gradient becomes sharper, which increases the drive for the drift waves.^{15–18}

The tearing mode is also considered to be the origin of the seed island for neoclassic tearing modes, which are dangerous modes in the future ITER experiments.¹⁹ To control these modes, one can modulate the current profile using lower hybrid current drive or electron cyclotron current drive to minimize the tearing mode drive.²⁰ Finally, in burning plasmas, energetic particles have been shown to stabilize the macro tearing mode in numerical simulations.^{21–23}

To understand these physics problems in tokomaks experiments, one needs to investigate carefully the properties of the tearing mode. However, the tearing mode is difficult to

be solved analytically because it is a nonlinear problem that is multi-scale in both time and space. As to the collisionless tearing mode, which is more relevant in high temperature plasmas, one needs to resolve the electron dynamics in the electron skin depth scale. Several physics models have been constructed for tearing mode simulations,^{24–26} which still need to overcome the severe numerical constraints of the fast electron motion. Noticing that the basic physics of the collisionless tearing mode can be introduced by the electron inertial in a fluid model, one only needs to calculate the electron inertial in the fluid model instead of describing the fast electron motion precisely with kinetic theory.²⁴ Higher order kinetic effects of electrons can then be incorporated perturbatively.

In a tokamak geometry, the gyrokinetic toroidal code (GTC) simulation of the resistive tearing mode has been carried out by retaining the resistivity in Ohm's Law.³ For the high temperature plasmas, the collisionless tearing mode may be more relevant than the resistive tearing mode. In this paper, we present in Section II the toroidal implementation of a finite-mass electron fluid model for the collisionless tearing mode, which is coupled to the gyrokinetic ions through gyrokinetic Poisson's equation and Ampere's law. Using the GTC,^{2,3,27–33} we have verified the linear behaviors of the collisionless tearing mode in cylindrical geometry where analytic results are available for verification of simulation results. The results of GTC simulations agree with analytic eigenvalue calculations, as shown in Section III. In Section IV, conclusions and future plans are given.

II. PHYSICS MODEL

Since the frequency and growth rate of tearing modes are much smaller than ion cyclotron frequency, we can utilize the nonlinear gyrokinetic simulation method,³⁴ which removes unwanted high frequency modes and rigorously retains all the linear and nonlinear wave-particle resonances and finite Larmor radius effects. In the low-beta plasmas where parallel magnetic perturbation can be neglected, the

^{a)}E-mail: zhihongl@uci.edu

gyrokinetic equation in canonical form for the species α of charged particles reads^{35,36}

$$\frac{\partial f_\alpha}{\partial t} + \dot{\mathbf{X}}_c \cdot \nabla f_\alpha + \dot{p}_\parallel \frac{\partial f_\alpha}{\partial p_\parallel} = 0, \quad (1)$$

$$\dot{\mathbf{X}}_c = \frac{1}{m_\alpha} \left(p_\parallel - \frac{q_\alpha}{c} \delta A_\parallel \right) \mathbf{b}_0 + \frac{c p_\parallel}{m_\alpha q_\alpha B_0} \left(p_\parallel - \frac{q_\alpha}{c} \delta A_\parallel \right) \nabla \times \mathbf{b}_0 + \frac{c \mathbf{b}_0}{q_\alpha B_0} \times \left[\nabla \left(\delta \phi - \frac{p_\parallel \delta A_\parallel}{m_\alpha c} \right) + \mu \nabla B_0 \right], \quad (2)$$

$$\dot{p}_\parallel = - \left(\mathbf{b}_0 + \frac{c}{q_\alpha B_0} p_\parallel \nabla \times \mathbf{b}_0 \right) \cdot \left[q_\alpha \nabla \left(\delta \phi - \frac{p_\parallel \delta A_\parallel}{m_\alpha c} \right) + \mu \nabla B_0 \right]. \quad (3)$$

Here, \mathbf{X}_c , p_\parallel , μ , m_α , and q_α denote gyrocenter position, the canonical parallel momentum, the magnetic moment, the mass, and the electric charge, and \mathbf{B}_0 , δA_\parallel , $\delta \phi$, and $\delta \mathbf{B}$ denote the equilibrium magnetic field, the perturbed parallel vector potential, the perturbed electrostatic potential, and

the perturbed magnetic field, respectively. $\mathbf{b}_0 = \frac{\mathbf{B}_0}{B_0}$ is the unit vector of equilibrium magnetic field, c and t denote the light speed and the time, and $\delta \mathbf{B} = \nabla \times \delta A_\parallel \mathbf{b}_0$. The electric potential $\delta \phi$ and parallel magnetic vector potential δA_\parallel are all gyro-averaged. Assuming that perturbed distribution function δf_α and equilibrium distribution function $f_{\alpha 0}$ satisfy $\delta f_\alpha / f_{\alpha 0} \sim o(\delta)$, we can solve the Vlasov equation above order by order

$$\frac{D}{Dt} f_\alpha = (L_0 + \delta L)(f_{\alpha 0} + \delta f_\alpha) = 0, \quad (4)$$

where

$$L_0 = \frac{\partial}{\partial t} + \left(\frac{p_\parallel}{m_\alpha} \mathbf{b}_0 + \frac{c p_\parallel^2}{m_\alpha q_\alpha B_0} \nabla \times \mathbf{b}_0 + \frac{c \mu}{q_\alpha B_0} \mathbf{b}_0 \times \nabla B_0 \right) \cdot \nabla - \left(\mathbf{b}_0 + \frac{c p_\parallel}{q_\alpha B_0} \nabla \times \mathbf{b}_0 \right) \cdot \mu \nabla B_0 \frac{\partial}{\partial p_\parallel}, \quad (5)$$

and

$$\delta L = \left\{ - \frac{q_\alpha \delta A_\parallel}{m_\alpha c} \left(\mathbf{b}_0 + \frac{c p_\parallel}{q_\alpha B_0} \nabla \times \mathbf{b}_0 \right) + \frac{c \mathbf{b}_0}{B_0} \times \left[\nabla \left(\delta \phi - \frac{p_\parallel \delta A_\parallel}{m_\alpha c} \right) \right] \right\} \cdot \nabla - \left(\mathbf{b}_0 + \frac{c p_\parallel}{q_\alpha B_0} \nabla \times \mathbf{b}_0 \right) \cdot q_\alpha \nabla \left(\delta \phi - \frac{p_\parallel \delta A_\parallel}{m_\alpha c} \right) \frac{\partial}{\partial p_\parallel}. \quad (6)$$

Here, $f_{\alpha 0}$ satisfies the 0th order of the above gyrokinetic equation

$$L_0 f_{\alpha 0} = 0, \quad (7)$$

which is approximated as a shift Maxwellian function

$$f_{\alpha 0} = \frac{n_{\alpha 0}}{(2\pi T_{\alpha 0} / m_\alpha)^{3/2}} \exp \left[- \frac{2\mu B_0 + m_\alpha (p_\parallel - v_{\parallel 0})^2}{2T_{\alpha 0}} \right].$$

The 1st order of the kinetic equation reads

$$L_0 \delta f_\alpha = - \delta L f_{\alpha 0} = \left\{ \frac{q_\alpha \delta A_\parallel}{m_\alpha c} \left(\mathbf{b}_0 + \frac{c p_\parallel}{q_\alpha B_0} \nabla \times \mathbf{b}_0 \right) - \frac{c \mathbf{b}_0}{B_0} \times \left[\nabla \left(\delta \phi - \frac{p_\parallel \delta A_\parallel}{m_\alpha c} \right) \right] \right\} \cdot \nabla f_{\alpha 0} + \left(\mathbf{b}_0 + \frac{c p_\parallel}{q_\alpha B_0} \nabla \times \mathbf{b}_0 \right) \cdot q_\alpha \nabla \left(\delta \phi - \frac{p_\parallel \delta A_\parallel}{m_\alpha c} \right) \frac{\partial}{\partial p_\parallel} f_{\alpha 0}. \quad (8)$$

If one uses the perturbative method to reduce the discrete particle noise, the evolution of the weight of perturbed distribution function for ion species $w_\alpha = \delta f_\alpha / f_\alpha$ satisfies

$$\frac{D w_\alpha}{Dt} = (1 - w_\alpha) \left\{ \left\{ \frac{q_\alpha \delta A_\parallel}{m_\alpha c} \left(\mathbf{b}_0 + \frac{c p_\parallel}{q_\alpha B_0} \nabla \times \mathbf{b}_0 \right) - \frac{c \mathbf{b}_0}{B_0} \times \left[\nabla \left(\delta \phi - \frac{p_\parallel \delta A_\parallel}{m_\alpha c} \right) \right] \right\} \cdot \frac{1}{f_{\alpha 0}} \nabla f_{\alpha 0} + \left(\mathbf{b}_0 + \frac{c p_\parallel}{q_\alpha B_0} \nabla \times \mathbf{b}_0 \right) \cdot q_\alpha \nabla \left(\delta \phi - \frac{p_\parallel \delta A_\parallel}{m_\alpha c} \right) \frac{1}{f_{\alpha 0}} \frac{\partial}{\partial p_\parallel} f_{\alpha 0} \right\}. \quad (9)$$

One can get the perturbed density and current by integrating the perturbed distribution

$$\delta n_x = \int \delta f_x d^3V,$$

$$\delta u_{x||c} = n_{0x} \int \frac{1}{m_x} p_{||} \delta f_x d^3V.$$

Since the electron gyroradius are much smaller than those of ions, the motion of electrons can be represented by the guiding center motions for electromagnetic waves with the wavelength on the order of ion gyroradius or collisionless skin depth D_e , which is much larger than ρ_e for typical fusion parameters. The gyrokinetic equation can be reduced to the drift kinetic equation for electrons. Integrating the linearized drift kinetic equation for the 0th and 1st order moments with the following tokamak plasmas ordering: $\nabla \ln(n_0) \sim 1/a$, $\nabla \ln(B_0) \sim 1/R$, $\nabla \ln(p_0) \sim 1/a$,^{3,24} and $a/R \ll 1$, one can derive the continuity and parallel momentum equation of electrons. We focus on linear formulation and simulation in this paper. The linearized continuity equation is

$$\begin{aligned} \frac{\partial \delta n_e}{\partial t} + \mathbf{B}_0 \cdot \nabla \left(\frac{n_{e0} \delta u_{e||}}{B_0} \right) + B_0 \mathbf{v}_E \cdot \nabla \left(\frac{n_{e0}}{B_0} \right) \\ - n_{e0} (\mathbf{v}^* + \mathbf{v}_E) \cdot \frac{\nabla B_0}{B_0} + \delta \mathbf{B} \cdot \nabla \left(\frac{n_{e0} u_{e||0}}{B_0} \right) \\ + \frac{c \nabla \times \mathbf{B}_0}{B_0^2} \cdot \left(-\frac{\nabla \delta p_{e||}}{e} + n_{e0} \nabla \delta \phi \right) = 0. \end{aligned} \quad (10)$$

The linearized parallel momentum equation is

$$\begin{aligned} m_e n_{e0} \frac{\partial \delta u_{e||c}}{\partial t} + q_e n_{e0} \mathbf{b}_0 \cdot \nabla \delta \phi + \mathbf{B}_0 \cdot \nabla \left(\frac{\delta P_{e||}}{B_0} \right) \\ + \delta \mathbf{B}_\perp \cdot \nabla \left(\frac{p_{e0}}{B_0} \right) = 0. \end{aligned} \quad (11)$$

Comparing with the perturbed parallel pressure terms, the perturbed perpendicular pressure terms are order of $O(1/k_\perp R_0)$ and thus can be neglected.³³ Assuming the electrons are isothermal along perturbed magnetic field line, one can make fluid closure to close the fluid model in magnetic flux coordinate as

$$\delta p_e = \delta n_e T_e + n_{e0} \delta \psi \frac{\partial}{\partial \psi} T_e + n_{e0} \delta \alpha \frac{\partial}{\partial \alpha} T_e, \quad (12)$$

where ψ is the poloidal magnetic flux, $\alpha = q\theta - \zeta$ is the magnetic field line label with poloidal angle θ and toroidal angle ζ , and $\delta\psi$ and $\delta\alpha$ are the perturbed parts of ψ and α , respectively.²⁸ The three equations above form a fluid electron model, which retains the electron inertial. Without considering the wave particle interaction, the model can describe the response of electron to the low frequency electromagnetic waves, such as the collisionless tearing mode, kinetic, and inertial Alfvén waves.^{24,37} In the electron fluid model above

$$\delta u_{e||} = \delta u_{e||c} - \frac{q_e \delta A_{||}}{m_e c}. \quad (13)$$

The perturbed $\mathbf{E} \times \mathbf{B}$ flow \mathbf{v}_E is

$$\mathbf{v}_E = \frac{c \mathbf{b}_0 \times \nabla \delta \phi}{B_0}. \quad (14)$$

And the diamagnetic flow \mathbf{v}^* is

$$\mathbf{v}^* = \frac{\mathbf{b}_0 \times \nabla (\delta P_\perp + \delta P_{||})}{n_{e0} m_e \Omega_{ce}}. \quad (15)$$

To calculate the higher-order wave particle interaction between the electromagnetic waves with the electron, one can make the closure of the electron fluid model kinetically by

$$\delta p_{||} = \int \frac{1}{m} p_{||}^2 \delta f d^3V, \quad (16)$$

$$\delta p_\perp = \int \mu B_0 \delta f d^3V, \quad (17)$$

where $\delta p_{||}$ and δp_\perp are parallel and perpendicular pressures, and the phase space integral represents

$$\int d^3V = \int \frac{2\pi B_0}{m^2} d\mu dp_{||}.$$

This kinetic closure is essentially a drift kinetic electron model, which needs to resolve the fast electron motion.

The background thermal ions and energetic particles can then be coupled to the fluid electrons through the Poisson's equation and Ampere's Law by

$$\frac{4\pi Z_i^2}{T_i} (\phi - \tilde{\phi}) = 4\pi \sum_\alpha n_\alpha q_\alpha. \quad (18)$$

$\tilde{\phi}$ is the second gyro-averaged electrostatic potential.³⁸

Together with the parallel Ampere's Law and the $k_{||} \ll k_\perp$ approximation

$$\left(\nabla_\perp^2 - \sum_\alpha \frac{\omega_{p\alpha}^2}{c^2} \right) \delta A_{||} = -\frac{4\pi}{c} \sum_\alpha n_{\alpha 0} q_\alpha \delta u_{\alpha||c}, \quad (19)$$

where $\omega_{p\alpha}$ is the plasma frequency of α species.

To verify the capability of this electron fluid model for the collisionless tearing mode without considering the ion's finite Larmor radius effects, we can write the Poisson's equation (18) into its long wave length limit

$$\frac{\rho_s^2}{\lambda_{De}^2} \nabla_\perp^2 \delta \phi = -4\pi \sum_\alpha \delta n_\alpha q_\alpha, \quad (20)$$

where λ_{De} is the electron Debye length. One should note that this simplification is not necessary in GTC simulation, the assumption made here is only for simplification of deriving the linear dispersion relation for the collisionless tearing mode below.

To derive the dispersion relation of the collisionless tearing mode in the fluid limit, one can derive the eigenvalue equation of $\delta A_{||}$ from Equations (11), (12), (19), and (20)

$$\begin{aligned} \nabla_\perp^2 \left(k_{||} v_{te}^2 - \frac{\omega^2}{k_{||}} \right) \nabla_\perp^2 \delta A_{||} = \nabla_\perp^2 \left(k_{||}'' v_{te}^2 - \frac{\omega^2 \omega_{pe}^2}{k_{||} c^2} \right) \delta A_{||} \\ + \frac{v_{te}^2}{\rho_s^2} \left(k_{||} \nabla_\perp^2 - k_{||}'' \right) \delta A_{||}, \end{aligned} \quad (21)$$

where k''_{\parallel} is the second derivative of parallel wave vector with respect to the minor radius, v_{te} is the thermal speed of electrons, and $\rho_s = \sqrt{T_e/(m_i\Omega_{ci})}$. The collisionless tearing mode is one of the eigenmodes of Equation (21). Separating Equation (21) into the inner electron inertial region and outer ideal MHD region and then asymptotically matching the solutions of the two regions, one can easily obtain the dispersion relation of the collisionless tearing mode.

Near the mode rational surface which locates at r_0 , in the inner electron inertial region ($r - r_0 \ll |\omega/k'_{\parallel}v_{te}|$), where non-ideal MHD effects resulting from the electron inertial play the role of magnetic field diffusive term in the evolution equation of the magnetic field, the equation above can be reduced to

$$\left(k''_{\parallel}v_{te}^2 - \omega^2\right) \frac{\partial^2}{\partial r^2} \delta A_{\parallel} = \left(-\frac{\omega^2\omega_{pe}^2}{c^2}\right) \delta A_{\parallel}. \quad (22)$$

While in the outer ideal MHD region ($r - r_0 \gg |\omega/k'_{\parallel}v_{te}|$), the equation reads

$$(k_{\parallel}\nabla_{\perp}^2 - k''_{\parallel})\delta A_{\parallel} = 0. \quad (23)$$

Matching the two regions near their boundaries

$$\Delta'_o = \lim_{|x|\rightarrow 0} \frac{\delta A'_{\parallel}}{\delta A_{\parallel}} = \Delta'_I = \lim_{|x|\rightarrow \infty} \frac{\delta A'_{\parallel}}{\delta A_{\parallel}}. \quad (24)$$

One can recover the growth rate for the collisionless tearing mode^{24,39}

$$-i\omega = \gamma = \frac{D_e^2}{\pi} |k'_{\parallel}v_{te}| \Delta'_o, \quad (25)$$

where D_e is the electron skin depth. Theoretically, one can recover the linear behavior of the collisionless tearing mode due to the electron inertial using this finite mass electron fluid model. Other non-ideal MHD effects may also lead to the magnetic reconnection, for example, the off-diagonal terms of electron pressure tensor in general Ohm's Law. Compared with the electron inertial, these terms are other of $O(\beta_e)$ term.⁴⁰ For conventional tokamak $\beta_e \sim 0.01$, these terms can be neglected for the collisionless tearing mode.

III. FLUID SIMULATION OF (2, 1) COLLISIONLESS TEARING MODE

Using the finite-mass electron fluid model, we have studied the linear properties of collisionless tearing modes, which might be relevant in high temperature tokamak plasmas.

A. Fluid simulation of the single (2, 1) collisionless tearing mode

Considering the uniform equilibrium pressure, we apply the q profile, $q = 1.8 + 100(r/R_0)^2$, where r is the minor radius, and use the parameters of inverse aspect ratio $\varepsilon = a/R_0 = 0.1$, major radius $R_0 = 1.68$ m, magnetic field $B_0 = 1.0$ T, equilibrium electron density on magnetic axis $n_{e0} = 10^{12}/\text{cm}^3$, and equilibrium electron beta $\beta_e = \frac{\rho_0}{8\pi B_0^2} = 0.00403$. With the

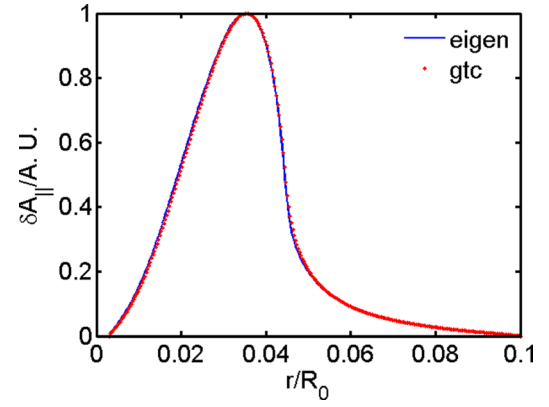


FIG. 1. Comparison of radial mode structures of the (2, 1) collisionless tearing mode from GTC simulation and 1D eigenvalue calculation in the cylindrical geometry.

realistic electron mass $m_e = 1837m_i$, the electron skin depth $D_e = 0.0032 R_0$, and the $\rho_s = 0.0061 R_0$, we get the mode structure of the single (2, 1) collisionless tearing mode from GTC simulation and eigenvalue calculation shown in Figs. 1 and 2.

Fig. 1 shows the typical (2, 1) single tearing mode structure. The mode structure from GTC simulation agrees with that from the eigenvalue calculation. Around the mode rational surface of $q = 2$ at $r = 0.045R_0$, there is a finite δA_{\parallel} , and the singularity of ideal MHD is resolved by the finite electron inertial. The corresponding 2D mode structures of δA_{\parallel} and $\delta\phi$ on the poloidal plane are shown in the left and right panels in Fig. 2.

In order to resolve the diffusive scale length D_e of the magnetic field, we use 300 grids in the minor radius domain of $[0.04a, a]$ in our simulation. For the simulation parameters above, in which $D_e = 0.0032R_0$, there are around 10 grid points in each D_e in the minor radius direction. One can achieve higher resolution by using more grids, which require more computing resource. To reduce the minor radius grid point, we have also tested the non-uniform grids to achieve higher resolution on the mode rational surface where the mode structure is steep. Using 150 grid points in minor radius direction, we have found the same mode structure and growth rate as those with the uniform grids.

For the specific parameters above, the growth rate of this (2, 1) single collisionless tearing mode from GTC simulation is $\gamma_{gtc} = 0.0001\Omega_{cp}$, which agrees well with the growth

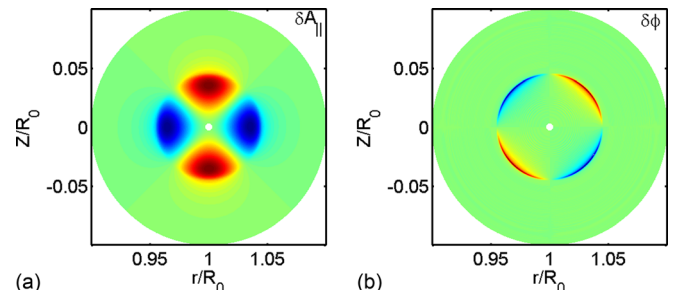


FIG. 2. Poloidal mode structures of δA_{\parallel} (left panel) and $\delta\phi$ (right panel) of the (2, 1) collisionless tearing mode from GTC simulation in the cylindrical geometry.

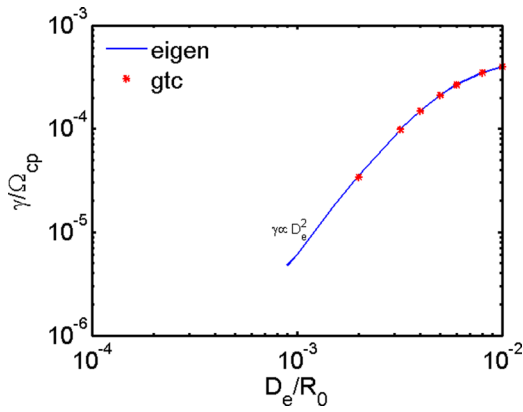


FIG. 3. The dependence of the growth rate γ of (2, 1) collisionless tearing mode on the electron skin depth D_e .

rate from eigenvalue calculation $\gamma_{\text{eig}} = 0.000098\Omega_{\text{cp}}$. We perform simulations with various D_e and find the scaling of the growth rate on D_e shown in Fig. 3.

Fig. 3 shows that the dependence of the single (2, 1) tearing mode growth rate γ on the electron skin depth D_e . In the small D_e regime, the growth rate approximately follows: $\gamma \propto D_e^2$, which agrees with the theoretic calculation $\gamma = \frac{b_2^2}{\pi} |k'_{\parallel} v_{te}| \Delta'_o$. Defining the inner region scale length as $x_e = |\frac{\gamma}{k'_{\parallel} v_{te}}|$, one can find $x_e \propto D_e^2$. The smaller D_e means smaller inner region and better scale separation between the inner and outer region. For the larger D_e , the inner region becomes larger and the scaling of the growth rate on D_e deviates from the theoretical prediction, which requires a large scale separation between inner and outer regions.²⁴

From the eigenvalue calculation using the finite-mass electron model verified in the current work, the growth rate of the (2, 1) single tearing modes as a function of D_e and ν_{ei} is shown in Fig. 4. We can see that in the pink circle where D_e is small and the collisional tearing mode dominates, the growth rate of (2, 1) single tearing mode depends on $\eta^{3/5}$.

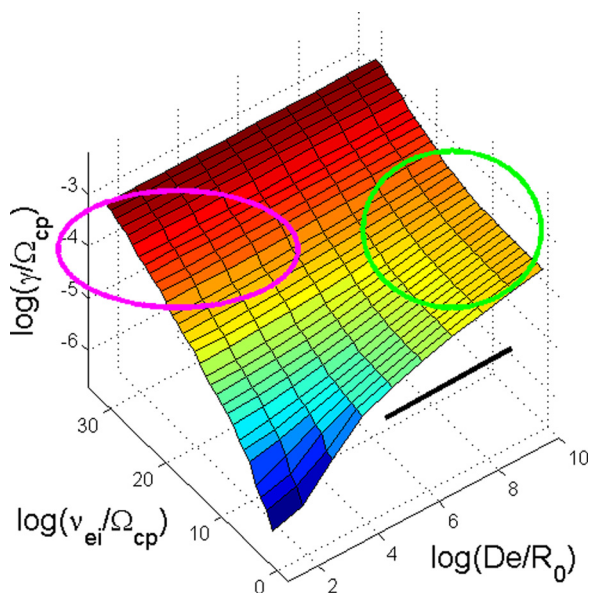


FIG. 4. The dependence of the growth rate γ of the (2, 1) single tearing mode on the electron skin depth D_e and resistivity from eigenvalue calculation.

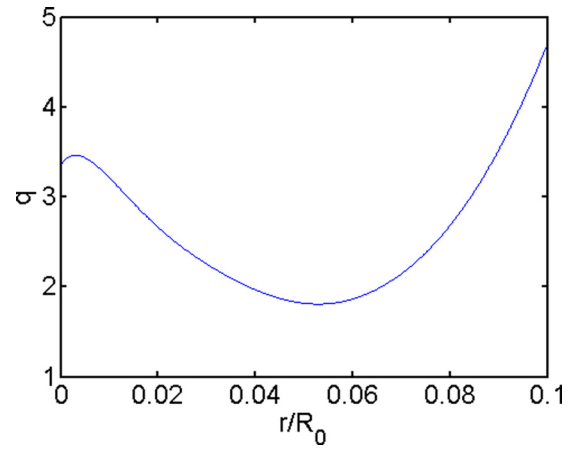


FIG. 5. Reversed q profile for (2, 1) double collisionless tearing mode simulation.

While in the green circle where electron-ion collision is weak, the collisionless tearing mode due to the finite electron inertial dominates, the growth rate of (2, 1) single tearing mode depends on D_e^2 . The discussion above indicates that with this electron fluid model, one can study both resistive and collisionless tearing modes.

B. Fluid simulation of (2, 1) double collisionless tearing mode

For the monotonous q profile above, the (2, 1) single collisionless tearing mode grows slowly. While for a reversed q profile, which might be relevant in the advanced tokamak discharge, the two (2, 1) single tearing modes may couple and result in a (2, 1) double tearing mode, which grows faster than the (2, 1) single tearing mode. So for model verification, we also simulate the (2, 1) double tearing mode.

Keeping the simulation parameters of the (2, 1) single collisionless tearing mode, but applying the reversed q profile shown in Fig. 5, we have investigated the (2, 1) double tearing mode with GTC simulation and eigenvalue calculation, as shown in Figs. 5 and 6.

In Fig. 6, most of the mode structure of the (2, 1) double tearing mode appears in the region $[0.38a, 0.68a]$. These two

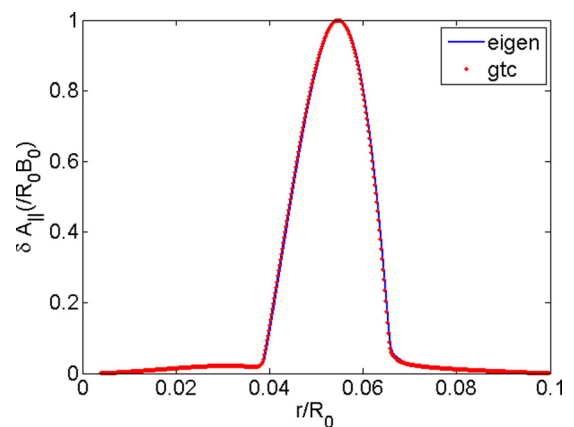


FIG. 6. Comparison of the radial mode structures of (2, 1) double collisionless tearing mode from GTC simulation and 1D eigenvalue calculation in the cylindrical geometry.

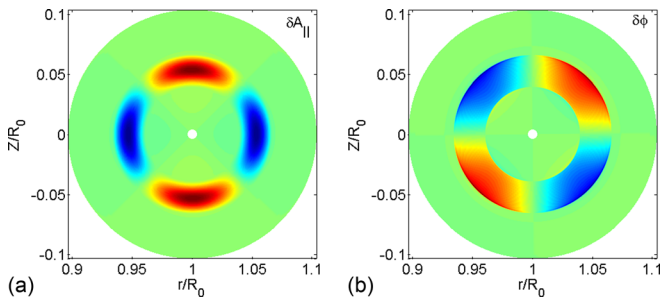


FIG. 7. Poloidal plane δA_{\parallel} (left panel) and $\delta\phi$ (right panel) mode structure of (2, 1) double collisionless tearing mode from GTC simulation in the cylindrical geometry.

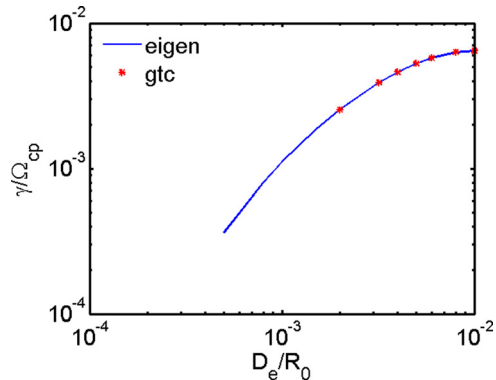


FIG. 8. The dependence of the growth rate γ of (2, 1) double collisionless tearing mode on the electron skin depth D_e .

points $r_1 = 0.38a$ and $r_2 = 0.68a$ are the positions of the $q = 2$ mode rational surfaces. This mode structure is the typical double tearing mode structure. The 2D mode structures on the poloidal plane are shown in Fig. 7. The radial profile of the electrostatic potential of the double tearing mode is much broader than that of the single tearing mode, which leads to a much larger growth rate of the double tearing mode. For this (2, 1) collisionless tearing mode, the growth rate from GTC simulation is $\gamma_{\text{gtc}} = 0.0040\Omega_{\text{cp}}$, which agrees well with the growth rate from eigenvalue calculation $\gamma_{\text{eig}} = 0.0039\Omega_{\text{cp}}$. The dependence of the growth rate of the (2, 1) double collisionless tearing mode on electron skin depth is shown in Fig. 8.

In Fig. 8, the growth rate of this (2, 1) double collisionless tearing mode in the limit of small D_e/R_0 approximately follows: $\gamma \propto D_e$, which is different from that of the (2, 1) single tearing mode. This scaling follows the calculation of Coppi *et al.*^{41,42} Since the (2, 1) double tearing mode is a global-type mode and the constant δA_{\parallel} approximation in the inner region does not hold, the scaling here is different from the scaling of the (2, 1) single tearing mode. Instead, the scaling here follows those of global-typed tearing modes, such as the (1, 1) tearing mode.

IV. SUMMARY

A finite-mass electron fluid simulation model is implemented in the GTC. The linear behaviors of both slowly growing single and fast growing double (2, 1) collisionless tearing modes have been verified. The good agreement

between GTC simulation and eigenvalue calculation demonstrates the capability of simulating collisionless tearing mode by GTC. Kinetic effects of thermal plasmas and energetic ions on the tearing modes, nonlinear evolution of the tearing mode, and nonlinear interaction between tearing mode and other Alfvén eigenmodes will be presented in future publications. The longer term plan for this work is to build a first-principles model and self-consistently simulate the neoclassical tearing mode in the core and micro-tearing mode in the pedestal of fusion plasmas.

ACKNOWLEDGMENTS

The first author appreciates helpful discussions with Y. Q. Liu. This work was supported by U.S. DOE SciDAC GSEP Center, China National Magnetic Confinement Fusion Science Program (Grant Nos. 2013GB111000, 2013GB112005, and 2015GB110004), and National Natural Science Foundation of China (Grant Nos. 11205109 and 11275162). This research used resources of the Oak Ridge Leadership Computing Facility at Oak Ridge National Laboratory (DOE Contract No. DE-AC05-00OR22725), and the National Energy Research Scientific Computing Center (DOE Contract No. DE-AC02-05CH11231).

- ¹H. P. Furth, J. Killeen, and M. N. Rosenbluth, *Phys. Fluids* **6**, 459 (1963).
- ²J. McClenaghan, Z. Lin, I. Holod, W. Deng, and Z. Wang, *Phys. Plasmas* **21**, 122519 (2014).
- ³D. Liu, W. Zhang, J. McClenaghan, J. Wang, and Z. Lin, *Phys. Plasmas* **21**, 122520 (2014).
- ⁴H. P. Furth, P. H. Rutherford, and H. Selberg, *Phys. Fluids* **16**, 1054 (1973).
- ⁵S. von Goeler, W. Stodiek, and N. Sauthoff, *Phys. Rev. Lett.* **33**, 1201–1203 (1974).
- ⁶T. Chapman, *Plasma Phys. Controlled Fusion* **53**, 013001 (2011).
- ⁷J. W. Connor, *Plasma Phys. Controlled Fusion* **40**, 531–542 (1998).
- ⁸J. F. Drake, N. T. Gladd, C. S. Liu, and C. L. Chang, *Phys. Rev. Lett.* **44**, 994–997 (1980).
- ⁹D. R. Hatch, D. Told, F. Jenko, H. Doerk, M. G. Dunne, E. Wolftrum, E. Viezzer, ASDEX Upgrade Team, and M. J. Pueschel, *Nucl. Fusion* **55**, 063028 (2015).
- ¹⁰Y.-T. Law, *Plasma Phys. Controlled Fusion* **38**, 1393–1396 (1996).
- ¹¹A. Biancalani, L. Chen, F. Pegoraro, and F. Zonca, *Phys. Rev. Lett.* **105**, 095002 (2010).
- ¹²A. Biancalani, L. Chen, F. Pegoraro, and F. Zonca, *Plasma Phys. Controlled Fusion* **53**, 025009 (2011).
- ¹³C. Wei, J. Xiaoquan, Y. Qingwei, D. Xuantong, L. Yi, F. Beibin, H. Yuang, L. Wei, Z. Yan, Z. Jun, S. Xianming, L. Liancai, D. Xuru, and HL-2A Team, *J. Phys. Soc. Jpn.* **79**, 044501 (2010).
- ¹⁴P. Buratti, P. Smealders, F. Zonca, S. V. Annibaldi, M. De Benedetti, H. Kroegler, G. Regnoli, O. Tudisco, and FTU-team, *Nucl. Fusion* **45**, 1446–1450 (2005).
- ¹⁵Z. Q. Hu, Z. X. Wang, L. Wei, J. Q. Li, and Y. Kishimoto, *Nucl. Fusion* **54**, 123018 (2014).
- ¹⁶Z. X. Wang, J. Li, Y. Kishimoto, and J. Q. Dong, *Phys. Plasmas (Letter)* **16**, 060703 (2009).
- ¹⁷S. Hu, J. Li, H. Qu, and Y. Kishimoto, *Phys. Plasmas* **21**, 102508 (2014).
- ¹⁸P. Jiang, Z. Lin, I. Holod, and C. Xiao, *Phys. Plasmas* **21**, 122513 (2014).
- ¹⁹R. J. Buttery, S. G. Gunter, G. Giruzzi, T. C. Hender, D. Howell, G. Huysmans, R. J. La Haye, M. Maraschek, H. Reimerdes, O. Sauter, C. D. Warrick, H. R. Wilson, and H. Zohm, *Plasma Phys. Controlled Fusion* **42**, B61–B73 (2000).
- ²⁰G. Giruzzi, M. Zabiégo, T. A. Gianakon, X. Garbet, A. Cardinali, and S. Bernabei, *Nucl. Fusion* **39**, 107 (1999).
- ²¹H. Cai and G. Fu, *Phys. Plasmas* **19**, 072506 (2012).
- ²²D. P. Brennan, C. C. Kim, and R. J. La Haye, *Nucl. Fusion* **52**, 033004 (2012).

- ²³H. Cai, S. Wang, Y. Xu, J. Cao, and D. Li, *Phys. Rev. Lett.* **106**, 075002 (2011).
- ²⁴D. Liu and L. Chen, *Plasma Phys. Controlled Fusion* **53**, 062002 (2011).
- ²⁵E. A. Sturdevant and W. W. Lee, *Phys. Plasmas* **21**, 022505 (2014).
- ²⁶W. A. Hornsby, P. Migliano, R. Buchholz, L. Kroenert, A. Weigl, A. G. Peeters, D. Zarzoso, E. Poli, and F. J. Casson, *Phys. Plasmas* **22**, 022118 (2015).
- ²⁷Z. Lin, T. S. Hahm, W. W. Lee, W. M. Tang, and R. B. White, *Science* **281**, 1835 (1998).
- ²⁸I. Holod, W. L. Zhang, Y. Xiao, and Z. Lin, *Phys. Plasmas* **16**, 122307 (2009).
- ²⁹Y. Xiao and Z. Lin, *Phys. Rev. Lett.* **103**, 085004 (2009).
- ³⁰W. Zhang, Z. Lin, and L. Chen, *Phys. Rev. Lett.* **101**, 095001 (2008).
- ³¹H. S. Zhang, Z. Lin, and I. Holod, *Phys. Rev. Lett.* **109**, 025001 (2012).
- ³²Z. Wang, Z. Lin, I. Holod, W. W. Heidbrink, and B. Tobias, *Phys. Rev. Lett.* **111**, 145003 (2013).
- ³³W. Deng, Z. Lin, and I. Holod, *Nucl. Fusion* **52**, 023005 (2012).
- ³⁴W. W. Lee, *Phys. Fluids* **26**, 556 (1983).
- ³⁵H. Naitou, K. Tsuda, W. W. Lee, and R. D. Sydora, *Phys. Plasmas* **2**, 4257 (1995).
- ³⁶A. J. Brizard and T. S. Hahm, *Rev. Mod. Phys.* **79**, 421 (2007).
- ³⁷D. Liu and L. Chen, *Phys. Scr.* **84**, 025506 (2011).
- ³⁸W. W. Lee, *J. Comput. Phys.* **72**, 243 (1987).
- ³⁹J. F. Drake and Y. C. Lee, *Phys. Fluids* **20**, 1341 (1977).
- ⁴⁰H. Cai and D. Li, *Phys. Plasmas* **16**, 052107 (2009).
- ⁴¹B. Coppi, *Phys. Lett.* **11**, 226 (1964).
- ⁴²B. Basu and B. Coppi, *Phys. Fluids* **24**, 465 (1981).